Folding and modulation of the helical conformation of Glycophorin A by point mutations†

Pei-Yin Lee,‡[a] Abhilash Sahoo [iD] ‡[b] and Silvina Matysiak [iD] *[c]

Transmembrane helix folding and self-association play important roles in biological signaling and transportation pathways across biomembranes. With molecular simulations, studies to explore the structural biochemistry of this process have been limited to focusing on individual fragments of this process – either helix formation or dimerization. While at an atomistic resolution, it can be prohibitive to access long spatio-temporal scales, at the coarse grained (CG) level, current methods either employ additional constraints to prevent spontaneous unfolding or have a low resolution on sidechain beads that restricts the study of dimer disruption caused by mutations. To address these research gaps, in this work, we apply our recent, in-house developed CG model (ProMPT) to study the folding and dimerization of Glycophorin A (GpA) and its mutants in the presence of Dodecyl-phosphocholine (DPC) micelles. Our results first validate the two-stage model that folding and dimerization are independent events for transmembrane helices and found a positive correlation between helix folding and DPC-peptide contacts. The wild type (WT) GpA is observed to be a right-handed dimer with specific GxxxG contacts, which agrees with experimental findings. Specific point mutations reveal several features responsible for the structural stability of GpA. While the T87L mutant forms anti-parallel dimers due to an absence of T87 interhelical hydrogen bonds, a slight loss in helicity and a hinge-like feature at the GxxxG region develops for the G79L mutant. We note that the local changes in the hydrophobic environment, affected by the point mutation, contribute to the development of this helical bend. This work presents a holistic overview of the structural stability of GpA in a micellar environment, while taking secondary structural fluctuations into account. Moreover, it presents opportunities for applications of computationally efficient CG models to study conformational alterations of transmembrane proteins that have physiological relevance.

1 Introduction

Integral membrane proteins play critical roles in signal transduction and transport across cell membranes.[1–4] The structure of these membrane proteins primarily feature tertiary structural arrangements such as a-helical and b-strand bundles or their combinations, with membrane spanning helix bundles being the dominant architecture.[5–7] Therefore, structure and relevant design implications of a-helix bundles are of significant interest to the research community to study their role in several physiological and pathological functions. Experimental and computational studies suggest that the formation of these membrane-spanning transmembrane helix bundles follows a two-step pathway.[8–11] First, the protein folds and inserts into the membrane, which allows it to bury the hydrophobic side-chains into the acyl core of the membrane. Then, the helix association occurs in this membranous environment, driven by a complex interplay of electrostatic and van der Waals effects. The folding of a solvated protein into a helical patch results in a free-energy gain, when the hydrogen-bonded polar backbone gets inserted into the membrane. Glycophorin A (GpA), found in human erythrocytes, is a well-studied benchmark for studies of transmembrane a-helices because of their functional relevance.[12–14] The structure of GpA in solution and solid state NMR have been well characterized.[15,16] GpA is a homodimer packing in a right handed fashion, where the contact surface between the two helices consist of an important motif GxxxG that is found to be critical in helix dimerization.[10,13,14] In order to understand the specific contacts allowing the formation of a stable helix dimer, mutational studies are essential as these

[a] Chemical Physics Program, University of Maryland, College Park, Maryland, USA

[b] Biophysics Program, University of Maryland, College Park, Maryland, USA

[c] Fischell Department of Bioengineering, University of Maryland, College Park, Maryland, USA. E-mail: matysiak@umd.edu; Tel: +1 301-405-0313

‡ P.-Y. L. and A. S. contributed equally to this work.

This journal is © the Owner Societies 2023

Phys. Chem. Chem. Phys., 2023, 25, 10885–10893 | 10885

studies enable us to locate interactions that are critical for dimer formation.

An early mutagenesis experiment, before the solution NMR structure of the GpA dimer was solved, established that GpA dimerization in detergent micelles is spontaneous and highly specific. Sensitive positions for mutations that would affect dimer stability were identified to occur every 3.9 residues, roughly co-located at the dimerization interface.[17] In addition, L75, I76, G79, G83, V84, and T87 were further identified as the most affected positions for point mutations. An alanine-scanning mutagenesis study further re-iterated that mutating residues at the dimer-interface led to significant disruption of dimer stability, especially at the ''GxxxG'' motif.[18] In this study, the authors also confirm that the hierarchy of the point mutation stability for GpA is independent of hydrophobic environments. Another FRET experiment has shown that for GpA in detergent micelles, helix formation is uncoupled from helix dimerization for both the wild type (WT) and mutant G79LG83L.[19] In this study, both the WT and mutant exhibit a a-helical signature in a far-UV circular dichroism spectra despite their dimerization status. These experimental results have suggested that the specific interactions occurring at the dimer surface are critical, and that designed mutants can modulate dimer stability. Fast local structural and environmental fluctuations can be crucial to self-association of GpA helices, particularly in a micellar environment. These dynamic effects can be significantly difficult to characterize through experimental methods because these methods often provide averaged information. On the other hand, molecular dynamics (MD) simulation methods can be leveraged to identify dynamic alterations that shape the protein structure and dimerization events.

The complete process of transmembrane helix formation and dimerization is still not feasible to simulate with atomistic simulations that use explicit expression for the solvent environment due to the long timescales required. Based on the two-stage model, the helix folding process and the dimerization event are independent so they can be investigated individually. Simulations on only dimerization (without focus on conformational changes) have been performed successfully to calculate free energies and association/dissociation rate calculations.[11,20,21] Moreover, CG simulations with the MARTINI forcefield of GpA in the DPPC bilayer can not only validate the experimental results on WT dimerization, but also study the disruption caused by mutations.[22–25] On the other hand, atomistic simulations with implicit representation of a membrane or detergent environment can be used to circumvent the issue on conformational transitions,[26] but at the expense of losing information of the interaction between the biomolecule and the solvent. Even though the folding process and the dimerization process can be studied separately, there are some circumstances in which the transmembrane helix conformational change is important and related to both processes (for example, when studying mutants). Conformational changes of transmembrane proteins can be important in enzyme activity. For example, it is reported that the structural and dynamical features of the helical transmembrane domain from the amyloid precursor protein (APP) are important in the proteolytic processing by g-secretase.[27] Mutation on the Gxxx-

GxxxG motif affects the helicity and changes the hydrophobic environment of the protein. In addition, the cleavage point is also affected.[27,28] These conformational variances cannot be studied with CG simulations that employ secondary structure constraints.[29,30] For the CG methods that do not apply constraints on secondary structures, for example the generic CG model developed by Bereau et al., the low resolution of the side chain beads could restrict the study of dimer disruption caused by point mutations.[31] In this work, we have used an in-house developed CG forcefield – ProMPT (Protein Model with Polarizability and Transferability) to study the impact of specific point-mutations on GpA folding and dimerization.[32] ProMPT can record accurate local environmental stimulus and institute protein's structural transitions. Therefore, this forcefield can be instrumental in deducing relationships between GpA/mutant's secondary structure and dimerization. In this article, we present a mechanistic overview on how mutations on GpA can modulate the conformational landscape of the transmembrane helices and their dimerization orientation. The point mutation at the GxxxG motif in the G79L mutant alters the local hydrophobic environment and results in a kink in the monomers. No dimerization is found for the G79L mutant and no specific contacts are found. For the T87L mutant, a high population of anti-parallel dimers are observed, possibly due to the lack of a T87–T87 lock.

2 Methods

2.1 GpA model

ProMPT features polar, non-polar and charged CG interaction sites, joined to create geometries specific to amino-acids, which are then used as building blocks to generate protein chains. The polar beads (such as the peptide backbone) have additional charged sites tethered to the central site, to introduce structural polarization, akin to the charge delocalization in real polar atomic species. The dipoles generated by the charged dummies in the backbone polar beads align themselves and shape the protein into a well-defined secondary structure. The mapping scheme for each amino acid and water is shown in Fig. S1 (ESI†). Previous publications have established the role of these added charges in structural transitions of the peptide backbone.[33–36] The interactions between CG sites are modelled to reproduce solvation, vaporization and partitioning free energies of the environment. Bonded interactions are developed to reproduce the distribution of individual bonded features from non-redundant protein structures in the protein data bank. The protein model is parametrized with the MARTINI polarizable water model.[37] More details on the model and validations can be found in our previous publication.[32]

Previous research has emphasized the importance of Ca–HO interactions in driving helix dimerization in membranous environments.[38,39] This allows polar amino-acids such as glycine to exist on dimerization surfaces. To capture the Ca–HO interactions in our low-resolution CG simulations, we have added an ad-hoc interaction between the main backbone

10886 | *Phys. Chem. Chem. Phys.*, 2023, 25, 10885–10893

This journal is © the Owner Societies 2023

bead of glycine with isoleucine and valine at the dimerization interface (Fig. S3, ESI†). The interaction is added as an inverted Gaussian function, with a median at 0.3 nm, and an amplitude and standard deviation of 15 kJ mol^{-1} and 0.2 nm respectively. The net well depth (B14.5 kJ mol^{-1} at 0.49 nm) of this Ca–HO interaction is close to the estimate from previous reported ab initio quantum calculations (B12.5 kJ mol^{-1}). Moreover the Ca–HO interaction we implemented in the model is an extremely short-ranged interaction, and the potential slowly approaches the initial LJ potential within 1 nm.

2.2   Dodecylphosphocholine (DPC) model

Since ProMPT is created with most of the interaction parameters along the MARTINI-defined interaction levels, it allows using the MARTINI forcefield for environmental entities, without any transferability issues. As such, the detergent molecules are created with the MARTINI forcefield. The mapping scheme for the DPC micelle is shown in Fig. S2 (ESI†). A tutorial on how to setup and perform the GpA simulations can be found at: https://www.matysiaklab.umd.edu/courses.html.

2.3   Simulation setup

All simulations are performed with GROMACS 2019.4.[40] A glycophorin A (GpA) WT monomer, with the sequence indicated in Fig. 1, is constructed as a random coil with VMD.[41] The resulting atomistic topology is then converted to a CG representation using an in-house code adopting the ProMPT model. The two resulting CG GpA monomers are then placed in parallel in an 8 nm wide cubic box with a center-of-mass distance of 5.66 nm between the two monomers. The box is then solvated with 80 DPC and 3000 CG water molecules. For mutants T87L and G79L (sequences shown in Fig. 1), the same work flow is followed with different starting mutated random coil structures. These CG structures are first energy minimized with the steepest descent algorithm. An NPT equilibration run at 350 K for 5 ns is followed at 1 bar and with a time step of 0.001 ps. The compressibility is 3.50 $\times$ 10^5 bar^{-1}. The production run in an NPT ensemble is then performed with a time step of 0.01 ps for the simulation time of 500 ns at 350 K. An electrostatic cutoff of 1.6 nm is used and the particle-mesh Ewald (PME) method is applied for the long range electrostatic interactions.[42,43] A Nose–Hoover thermostat is used to maintain the system at the desired temperature.[44] Six replicas are run for each WT/mutant.

2.4   Analyses

We use potential of mean force (PMF) plots to capture the conformational landscape for GpA WT and mutants. For each replica, only the trajectory after at least one intermonomer primary CG site (any CG interaction site that is not a dummy) contacts with a cutoff of 6 Å is used for analysis. The PMF was calculated by aggregating data from six replica simulations, binning the collective-variables and mapping the probabilities to PMF with $-k_bT \log(P_i)$, where P_i is the probability of finding the conformations in the ith bin. The average helical content and the number of backbone (BB) contacts are used as the reaction coordinates for the PMF calculations. Helical content is defined as the fraction of intramonomer backbone contacts with a cutoff of 6.5 Å, that are native to the PDB-converted-CG structure (PDB code: 1AFO.pdb). For calculating the number of inter-monomer backbone contacts, we also used a cutoff of 6.5 Å Configurations from the most populated basin of the PMF plots for each WT and mutant is extracted and used for all the following analyses. The criteria to determine the most populated basin, informed from the computed PMFs, is 0.95–1 (average helical content) and 9–18 (number of inter-monomer BB contacts), 0.95–1 (average helical content) and 14–22 (number of inter-monomer BB contacts), and 0.85–0.92 (average helical content) and 6–12 (number of inter-monomer BB contacts) for WT, T87L, and G79L, respectively. For the crossing angle computation, only the BB is considered. The crossing angle is determined by two vectors, where each vector only considers the position of the tail and the head of the monomer. The contact map is constructed by counting the contacts between intermonomer BB with a cutoff of 6.5 Å and dividing by the total number of frames used for analysis. As for the average number of DPC contacts, a contact is counted when the desired bead (Choline: NC3 or acyl-tails: C3) is within 6 Å of any CG beads from the GpA peptides (calculated from the first peak of radial-distribution-function) and then divided by the total number of frames used for analysis. Only the BB is considered when calculating the dihedral angle for G79L. All the insert GpA images are rendered with Visual Molecular Dynamics (VMD).

3   Results and discussion

3.1   Helix formation is not coupled with dimerization

As shown in Fig. 2 and from other trials presented in the ESI,† peptide helicity increases as the number of DPC-peptide contacts increases, exhibiting a positive correlation. From this result, no causal relationship can be inferred (that is, it cannot be concluded whether DPC helps helix formation or helix formation attracts more DPC molecules near the peptides). Full helices are observed before the peptides start to dimerize. This observation agrees with previous findings that helix formation and dimerization are independent processes.[8–11]

3.2   Conformational landscape of GpA and mutants

As validation of our model and to establish comparisons with previous experimental and simulation results, we computed the potential of mean force (PMF). Fig. 3a shows the PMF of WT GpA, where the most populated basin is observed with a high average helical content and a broad range for the number of

Fig. 1   The amino acid sequence for WT, T87L, and G79L. The mutation point is in red and the GxxxG motif is underlined. The residue index is also marked on the top.
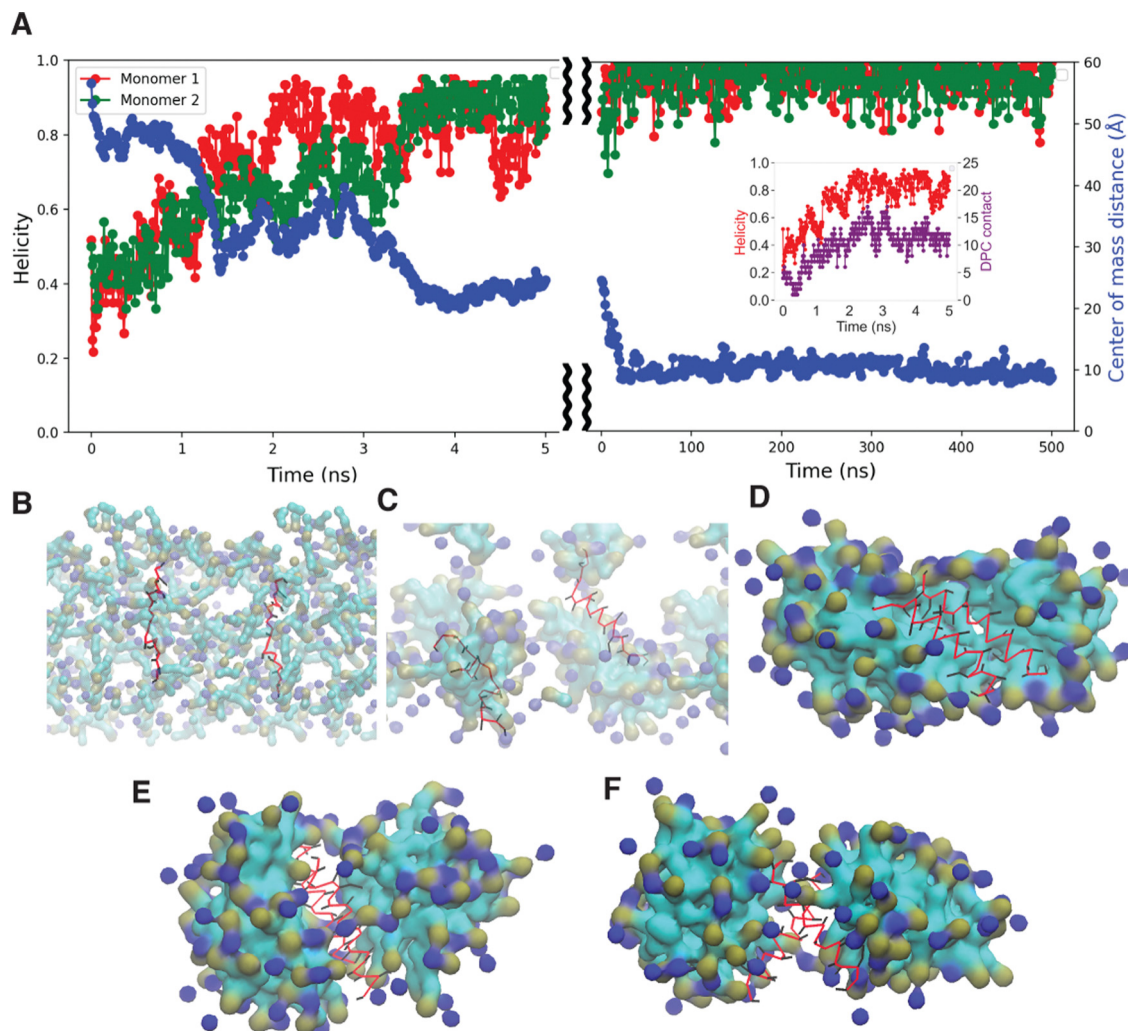
Fig. 2   (A) Time series of helicity for two WT GpA peptides and the center of mass distance between these two peptides. The inset shows the time series for helicity of one WT GpA peptide and its DPC contacts. (B) The initial frame with peptide (in red and black) co-solvated with DPC molecules. (C) Peptides conform into helical structures before associating (frame at 5 ns). (D) Peptide assembly on the surface of the micelle (frame at 25 ns). (E and F) Assembled peptide inserted into the micelle (frame at 207 ns).

inter-monomer BB contacts. A representative conformation is shown as the inset figure. In this representative conformation, the WT GpA dimerizes as a parallel dimer with T87–T87 interaction. This T87–T87 interaction can also be seen in the contact map between the two monomers (Fig. 4a). In addition, the GxxxG motif of the two monomers also have contacts with each other (see also Fig. 4a). These structural features agree with the solution NMR structures solved in the DPC micelles where extensive backbone–backbone contacts are found within the G79/G83 region.[15] It has been reported from mutational analysis that there is a high specificity of sequence dependence on GpA dimerization.[17] We first examine the mutant T87L where dimer disruptions have been reported for any non-polar amino acid as a replacement of T87.[17] The most populated basin in the PMF of mutant T87L (Fig. 3b) spans a range of average helical content that is similar to that of WT, but with a higher number of inter-monomer BB contacts. A second populated basin is observed with similar high helical content

but with a lower number of inter-monomer BB contacts. The conformations in these two basins can dimerize in both parallel and anti-parallel fashion (Fig. 4b). The insert of Fig. 3b shows a representative conformation for a parallel T87L dimer. In this parallel T87L dimer, the critical T87–T87 interaction existing in the WT dimer is disrupted by the substitute Leu residues. These Leu residues rather interact with the DPC molecules and not between themselves, which is in contrast to the interaction between Thr residues at this position for the WT. The GxxxG motif is observed to have contacts with each other (Fig. 4b). Lastly we examine the mutant G79L, which has also been reported from mutational experiments to form monomers.[17] From Fig. 3c we observe the most populated basin in the PMF to have a lower range of average helicity content compared to that of the WT and T87L. The number of inter-monomer BB contacts also decreases. We note a bent-helix for one of the monomers (insert Fig. 3c), and the dimer does not have T87–T87 interactions as observed in the contact
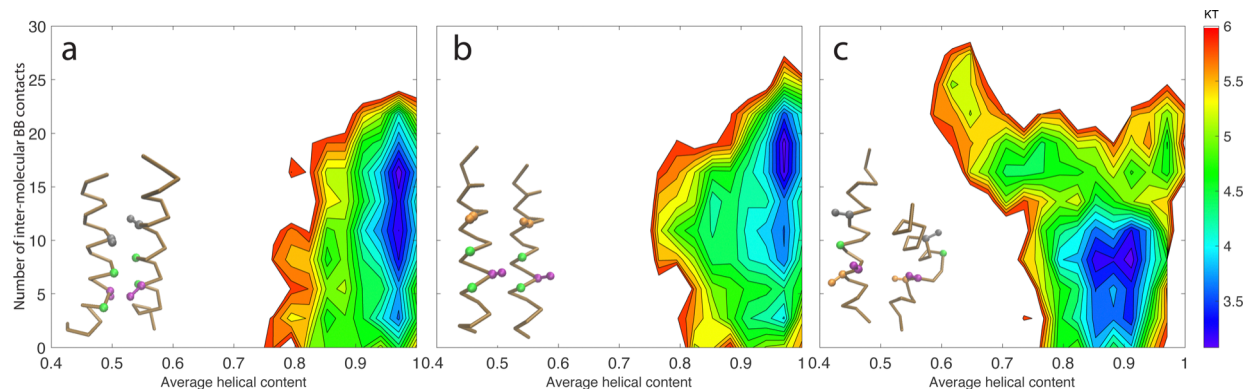
Fig. 3 PMF for (a) WT, (b) T87L, and (c) G79L GpA with the average helical content and the number of inter-monomer BB contacts as the reaction coordinates. The criteria to determine the most populated basin is 0.95 to 1 (average helical content) and 9 to 18 (number of inter-monomer BB contacts), 0.95 to 1 (average helical content) and 14 to 22 (number of inter-monomer BB contacts), and 0.85 to 0.92 (average helical content) and 6 to 12 (number of inter-monomer BB contacts) for WT, T87L, and G79L, respectively. The representative conformation for each WT/mutant is shown in the inset figures. Color code: Thr (grey), Gly (green), Val (purple), and Leu (orange).
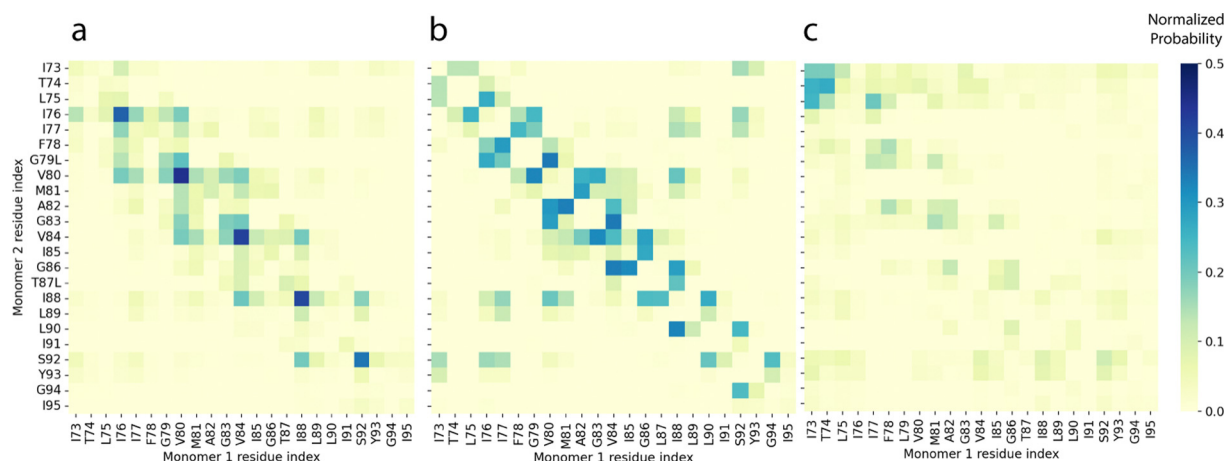

Fig. 4 The residue–residue contact maps for (a) WT, (b) T87L, and (c) G79L.

map of G79L (Fig. 4c). Moreover, since G79 is mutated to a Leu residue, the original GxxxG motif does not exist and there are no intermonomer contacts between the same region of the monomers. The same decrease in inter-monomer interaction has also been reported in a previous biological membrane experiment for mutant G79I.[10]

3.3 Changes in peptide-surfactant interactions tune the emergence of helix bend formation

We further inspect the reasons for the monomer-bending in G79L by examining the contacts between G79L and DPC detergent micelles. Fig. 5a shows the average number of contacts between each WT/G79L residue and DPC headgroup (NC3). The major difference between the WT and G79L occurs at the middle part of the monomer, where there are more residue-NC3 contacts for G79L, especially for residue V80 to V84, which belong to the GxxxG motif. Fig. 5b shows similar analysis but with the hydrophobic bead (C3) of DPC. In this case, the residues at the central region of the G79L mutant are

less exposed to C3, especially for M81 and I85. Moreover, we note that the mutated L79 has more contacts with C3, driven by the hydrophobic effect, and this alters the following six residues (V80 to I85) to be more exposed to the DPC headgroup which is closer to the micelle/water interface. Subtle changes in the hydrophobic environment caused by a point mutation were also observed in previously published literature, where a mutation point at the GxxxG motif of Amyloid Precursor Protein (APP) results in a different hydration level of the transmembrane protein compared to the WT.[27] The change in the hydrophobic environment near the center of the G79L mutant potentially destroys the hydrophobicity balance in the original helix and results in a helical bend.

3.4 Increased helical flexibility near the GxxxG region

The dihedral angle analysis for G79L (Fig. 6) provides a quantitative analysis for the bending region of the G79L mutant. From residues L79 to G86, we observe large deviations in the dihedral angle, which marks a hinge in the a-helix. This result agrees

This journal is © the Owner Societies 2023

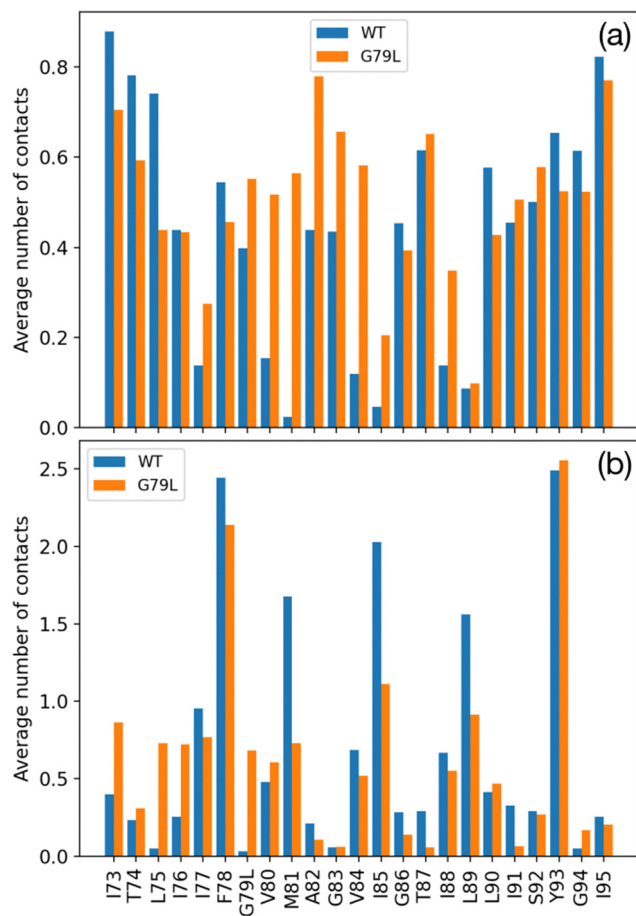*Phys. Chem. Chem. Phys.*, 2023, 25, 10885–10893 | 10889

Fig. 5   The average number of contacts between WT (blue)/G79L (orange) and the (a) choline bead (NC3) and (b) hydrophobic bead (C3) of the DPC detergent.
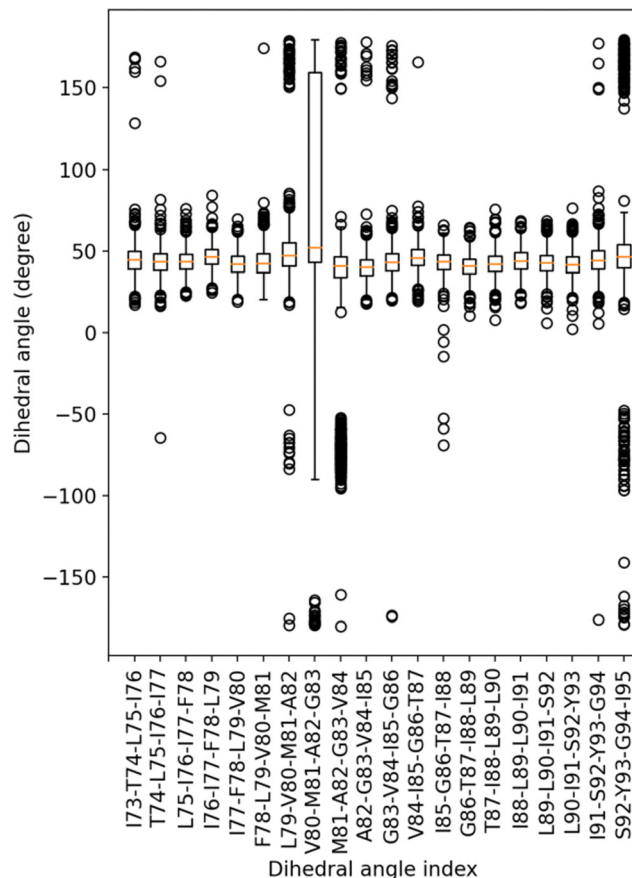

Fig. 6   Dihedral angle analysis for G79L, where the x-axis shows the dihedral angle index and the y-axis shows the dihedral angle. The median is shown in orange, the box includes the interquartile range, the bars show the positions of minimum and maximum, and the circles are the outliers.

with the previous residue-DPC contact analyses where the same region experiences the most significant environmental variation resulting in a bent conformation. The position of the hinge at the GxxxG region agrees with previous findings for mutated APP where bending and modulation of helicity is observed at the GxxxG region.[27,28] Lemmin et al. noted a loss in helicity and helical bending due to a mutation of Gly to Leu at the N-terminal side of the GxxxGxxxG domain, similar to our observation for GpA. On the other hand, Gotz et al. found an increase in helicity if the Gly to Leu mutation is at the C-terminal side, which shows that the change of transmembrane helix helicity is also a function of where the mutation is performed in the GxxxG motif. The characterization of transmembrane protein helix bending is important because the structural and dynamical variance caused by point mutations could result in different enzymatic activity and dimer stability. Since the a-helix is bent but not destroyed, high helicity can still be expected. A similar, but more disruptive GpA double mutant G79LG83L has been reported to still exhibit an a helical secondary structure from circular dichroism (CD) data.[19] Therefore, we hypothesize that CD cannot precisely distinguish this slight loss in helicity originating from monomer bending, since the average helicity from simulations is still high (around 90%) (Fig. 3c) for G79L.

In the case of GpA, unlike soluble coils where the formation of the helix is coupled to dimerization, the formation of a-helices and dimerization are independent events.[8] For the WT the helices are stable due to the strong hydrogen bonding in a low dielectric environment and the formation of the dimer can be stabilized by van der Waals' interactions between complementary surfaces of the two TM helices.[19,45] However, for G79L, the mutation of Gly to Leu results in a bent a-helix which does not have a smooth surface at the GxxxG region to aid close backbone interactions. In our model, compared to the popular MARTINI CG model, there are no specific secondary structure restraints imposed, and therefore folding transitions can be observed. This allows us to explore the helix bending for the G79L mutant, which could not be captured with previous CG forcefields.

3.5 Crossing angle analysis shows the difference in parallel dimer and anti-parallel dimer population

To characterize the relative orientations of the dimer population, we use the helix crossing angles between the monomers. In Fig. 7, the majority of the crossing angles for the WT GpA spans a range of ÿ50 to 201. This broad range of crossing angles comes from a variety of packing orientations, which could explain the large variation in the number of inter-monomer

BB contacts from Fig. 3 due to different packing fashions. In our simulation, most of the WT GpA dimers are right-handed, indicated by a negative helix crossing angle. A skewed bimodal distribution for the crossing angle is observed for the WT, which agrees with previous CG simulation results performed in a lipid membrane.[22] The collection of vertical lines centered around ÿ401 in Fig. 7 marks the crossing angles of the solution NMR GpA dimer structures[15] reported in the PDB. The deviation in crossing angles between the NMR structure and our results could come from the "softer" nature of CG models due to a smoothed free energy surface, which has also been noted in previous CG simulations.[22] While few in number, we also recorded some anti-parallel dimers for the WT GpA, which have an absolute crossing angle larger than around 1501. Anti-parallel dimers have been reported before in atomistic simulations with implicit membrane and implicit cyclohexane.[46] These dimers could have comparable energy to that of a native dimer. In cyclohexane, there is a higher probability of observing anti-parallel dimers compared to membranes due to a lack of directional barrier preventing parallel-anti-parallel dimer flipping. From the residue–residue contacts in the contact map (Fig. 4a), it can be noted that the dimers are highly symmetric and specific. This specificity of contact surface was also observed in earlier CG simulations in a membrane environment where a mobile helix was anisotropically distributed near another fixed helix,[22] with specificity originating from the close contacts at the GxxxG motif.

Fig. 7 shows the distribution of T87L crossing angles in green. Compared to the crossing angles for WT, the crossing angles for T87L deviate more from the solution NMR structures with a range of ÿ35 to 251. Within this region, parallel dimers with a crossing angle near 01 are more populated, which could explain the higher number of inter-monomer BB contacts observed from the PMF of T87L, because the monomers are more parallel to each other and create more contacts. However, comparing the total parallel dimer probability (absolute crossing angle less than 501), it is still more probable to have parallel dimers in the case of the WT. On the other hand, a significant fraction of dimers observed for T87L are anti-parallel, much higher than for WT. The GxxxG contact is also observed for the parallel T87L dimers (Fig. 4b), but in a more diffused fashion. While the GxxxG motif contributes largely to the dimerization of the GpA monomers, it is also reported that two thirds of the stabilizing intermonomer energy comes from outside the GxxxG motif.[46] In this case, the lack of the original T87–T87 interaction could be a reason why the parallel dimer is less sampled in the most populated basin for T87L compared to WT, as T87 has been reported to involve hydrogen bonding between helices and help dimer stabilization.[47,48] T87L has been reported to form little to no dimers in a sodium dodecyl sulfate polyacrylamide gel electrophoresis (SDS-PAGE) experiment,[17] but in our simulations we observe the formation of some parallel dimers with a lower probability compared to that for the WT. In a previous analytical ultracentrifugation study, mutants that are reported to be disruptive in SDS-PAGE experiment are observed to still form significant dimers in detergent C_8E_5 micelles, but less than WT.[49] In addition, in previous CG GpA simulations, the disruptive mutants reported by SDS-PAGE experiment are also observed with a significant amount of dimers in lipid membranes.[22,25] It could be that with the SDS-PAGE experiment, the population of dimers is too low to capture. Our results agree qualitatively that parallel dimers for T87L are less stable than the WT dimers.

Finally, a much broader distribution of the crossing angles is observed for G79L due to the bent structure of individual monomers. The contact map for G79L further confirms the fact that there is no specific interactions between the two monomers (Fig. 4c). Compared to the WT and T87L mutant, the contact map for G79L is significantly more diffusive with only observable contacts between the N-terminus of the two monomers.

3.6 Conclusion

Although the two-stage model for transmembrane helices allows independent investigations on helix folding and helix dimerization, simulations that can examine folding-dimerization simultaneously can present a holistic overview of environment-effected modulations to helix formation, dimerization and their interplay. In this work, we apply a newly developed CG model ProMPT to investigate glycophorin A (GpA) transmembrane folding in micellar conditions from random coils to dimerization and found a positive correlation of helix folding with an increase of DPC–peptide interactions. We validate the two-stage model in which helix formation is not coupled with GpA dimerization. In addition, we also look at the dimer stability for GpA WT and two mutants. In our initial validations with the WT GpA, we observe several structural characteristics that were previously explored in the literature such as the GxxxG contacts and the helix crossing angle. We explored the structural stability of the helical dimers through specific point mutations aimed at isolating individual
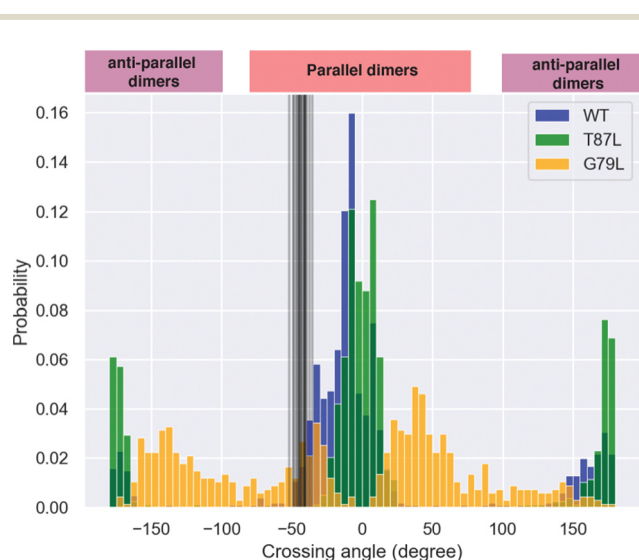

Fig. 7 The crossing angle distribution for WT (blue), T87L (green), and G79L (orange). The x-axis is the crossing angle in degree. The y-axis is the probability of observing a specific crossing angle for the WT or the mutant. The black vertical lines represent the crossing angles from the 20 NMR fitted structures in the PDB structure (1AFO.pdb). An approximate extent of parallel and antiparallel dimer arrangements is provided at the top.

This journal is © the Owner Societies 2023

Phys. Chem. Chem. Phys., 2023, 25, 10885–10893 | 10891

interactions at the GxxxG region (G79L) and hydrogen bonding at the C-terminus (T87L). From the PMF plots, T87L could form helical dimers, but G79L loses some helicity, and could not form stable helical dimers. We find that point mutations at the GxxxG motif alter the local hydrophobic environment and contribute to helix bending through a hinge at the GxxxG region. A similar hinge structure at GxxxG has been previously reported for APP. But, even with the hinge we still observe high helicity (B90%) for G79L monomers. A significant fraction of WT exhibits right-handed dimer conformation, while there are more anti-parallel dimers observed for T87L, possibly due to a lack of the T87–T87 lock. For G79L, there are no specific crossing angles observed as there are no stable dimers. In addition, more diffused contacts between monomers suggest a decrease in dimerization specificity. The ability to capture this secondary structure change is a novelty of the ProMPT model which cannot be studied with previous CG models where restraints on secondary structures are imposed. This opens up future possibilities to use foldable and transferable CG models to understand conformational fluctuations and the impact of point mutations in physiological transmembrane proteins, where local environmental fluctuations can play a key role.

Conflicts of interest

There are no conflicts to declare.

Acknowledgements

References

1 S. Cowan and J. P. Rosenbusch, Folding pattern diversity of integral membrane proteins, Science, 1994, 264, 914–916.

2 K. S. Song, S. Li, T. Okamoto, L. A. Quilliam, M. Sargiacomo and M. P. Lisanti, Copurification and Direct Interaction of Ras with Caveolin, an Integral Membrane Protein of Caveolae Microdomains: Detergent-free Purification of Caveolae Membranes, J. Biol. Chem., 1996, 271, 9690–9697.

3 P. J. Robinson, Signal transduction by GPI-anchored membrane proteins, GPI Membr. Anchors, 1991, 22–28.

4 B. Mertz, A. V. Struts, S. E. Feller and M. F. Brown, Molecular simulations and solidstate NMR investigate dynamical structure in rhodopsin activation, Biochim. Biophys. Acta, Biomembr., 2012, 1818, 241–251.

5 I. T. Arkin, Structural aspects of oligomerization taking place between the transmembrane a-helices of bitopic membrane proteins, Biochim. Biophys. Acta, Biomembr., 2002, 1565, 347–363.

6 H. Viklund, E. Granseth and A. Elofsson, Structural classification and prediction of reentrant regions in a-helical transmembrane proteins: application to complete genomes, J. Mol. Biol., 2006, 361, 591–603.

7 M. Hong, Y. Zhang and F. Hu, Membrane protein structure and dynamics from NMR spectroscopy, Annu. Rev. Phys. Chem., 2012, 63, 1.

8 J.-L. Popot and D. M. Engelman, Membrane protein folding and oligomerization: the two-stage model, Biochemistry, 1990, 29, 4031–4037.

9 J.-L. Popot and D. M. Engelman, Helical membrane protein folding, stability, and evolution, Annu. Rev. Biochem., 2000, 69, 881–922.

10 C. Finger, T. Volkmer, A. Prodohl, D. E. Otzen, D. M. Engelman and D. Schneider, The stability of transmembrane helix interactions measured in a biological membrane, J. Mol. Biol., 2006, 358, 1221–1228.

11 J. Henin, A. Pohorille and C. Chipot, Insights into the recognition and association of transmembrane a-helices. The free energy of a-helix dimerization in glycophorin A, J. Am. Chem. Soc., 2005, 127, 8478–8484.

12 H. I. Petrache, A. Grossfield, K. R. MacKenzie, D. M. Engelman and T. B. Woolf, Modulation of glycophorin A transmembrane helix interactions by lipid bilayers: molecular dynamics calculations, J. Mol. Biol., 2000, 302, 727–746.

13 W. P. Russ and D. M. Engelman, The GxxxG motif: a framework for transmembrane helix-helix association, J. Mol. Biol., 2000, 296, 911–919.

14 B. Brosig and D. Langosch, The dimerization motif of the glycophorin A transmembrane segment in membranes: importance of glycine residues, Protein Sci., 1998, 7, 1052–1056.

15 K. R. MacKenzie, J. H. Prestegard and D. M. Engelman, A transmembrane helix dimer: structure and implications, Science, 1997, 276, 131–133.

16 S. O. Smith, D. Song, S. Shekar, M. Groesbeek, M. Ziliox and S. Aimoto, Structure of the transmembrane dimer interface of glycophorin A in membrane bilayers, Biochemistry, 2001, 40, 6553–6558.

17 M. A. Lemmon, J. M. Flanagan, H. R. Treutlein, J. Zhang and D. M. Engelman, Sequence specificity in the dimerization of transmembrane. alpha.-helixes, Biochemistry, 1992, 31, 12719–12725.

18 K. G. Fleming and D. M. Engelman, Specificity in transmembrane helix–helix interactions can define a hierarchy of stability for sequence variants, Proc. Natl. Acad. Sci. U. S. A., 2001, 98, 14340–14344.

19 L. E. Fisher, D. M. Engelman and J. N. Sturgis, Detergents modulate dimerization, but not helicity, of the glycophorin A transmembrane domain, J. Mol. Biol., 1999, 293, 639–651.

20 J. Domanski, M. S. Sansom, P. J. Stansfeld and R. B. Best, Atomistic mechanism of transmembrane helix association, PLoS Comput. Biol., 2020, 16, e1007919.

21 J. Domanski, M. S. Sansom, P. J. Stansfeld and R. B. Best, Balancing force field protein–lipid interactions to capture transmembrane helix–helix association, J. Chem. Theory Comput., 2018, 14, 1706–1715.

22 E. Psachoulia, P. W. Fowler, P. J. Bond and M. S. Sansom, Helix- helix interactions in membrane proteins: Coarse-

10892 | Phys. Chem. Chem. Phys., 2023, 25, 10885–10893

This journal is © the Owner Societies 2023

grained simulations of glycophorin A helix dimerization, Biochemistry, 2008, 47, 10503–10512.

23 S. J. Marrink, H. J. Risselada, S. Yefimov, D. P. Tieleman and A. H. de Vries, The MARTINI Force Field: Coarse Grained Model for Biomolecular Simulations, J. Phys. Chem. B, 2007, 111, 7812–7824.

24 L. Monticelli, S. K. Kandasamy, X. Periole, R. G. Larson, D. P. Tieleman and S.-J. Marrink, The MARTINI Coarse-Grained Force Field: Extension to Proteins, J. Chem. Theory Comput., 2008, 4, 819–834.

25 T. A. Wassenaar, K. Pluhackova, A. Moussatova, D. Sengupta, S. J. Marrink, D. P. Tieleman and R. A. Bockmann, High-throughput simulations of dimer and trimer assembly of membrane proteins. The DAFT approach, J. Chem. Theory Comput., 2015, 11, 2278–2291.

26 J. P. Ulmschneider and M. B. Ulmschneider, Folding simulations of the transmembrane helix of virus protein U in an implicit membrane model, J. Chem. Theory Comput., 2007, 3, 2335–2346.

27 T. Lemmin, M. Dimitrov, P. C. Fraering and M. Dal Peraro, Perturbations of the straight transmembrane a-helical structure of the amyloid precursor protein affect its processing by g-secretase, J. Biol. Chem., 2014, 289, 6763–6774.

28 A. Gotz, N. Mylonas, P. Hogel, M. Silber, H. Heinel, S. Menig, A. Vogel, H. Freyrer, D. Huster and B. Luy, et al., Stabilization/destabilization of the app transmembrane domain by mutations in the diglycine hinge alter helical structure and dynamics, and impair cleavage by-secretase, bioRxiv, 2018, 10.

29 S. Kawamoto, H. Liu, Y. Miyazaki, S. Seo, M. Dixit, R. DeVane, C. MacDermaid, G. Fiorin, M. L. Klein and W. Shinoda, SPICA Force Field for Proteins and Peptides, J. Chem. Theory Comput., 2022, 18, 3204–3217.

30 S. J. Marrink, H. J. Risselada, S. Yefimov, D. P. Tieleman and A. H. De Vries, The MARTINI force field: coarse grained model for biomolecular simulations, J. Phys. Chem. B, 2007, 111, 7812–7824.

31 T. Bereau and M. Deserno, Generic coarse-grained model for protein folding and aggregation, J. Chem. Phys., 2009, 130, 06B621.

32 A. Sahoo, P.-Y. Lee and S. Matysiak, Transferable and Polarizable Coarse Grained Model for Proteins—ProMPT, J. Chem. Theory Comput., 2022, 18(8), 5046–5055.

33 S. J. Ganesan and S. Matysiak, Role of backbone dipole interactions in the formation of secondary and supersecondary structures of proteins, J. Chem. Theory Comput., 2014, 10, 2569–2576.

34 S. J. Ganesan, H. Xu and S. Matysiak, Effect of lipid head group interactions on membrane properties and membrane-induced cationic b-hairpin folding, Phys. Chem. Chem. Phys., 2016, 18, 17836–17850.

35 A. Sahoo, H. Xu and S. Matysiak, Pathways of amyloid-beta absorption and aggregation in a membranous environment, Phys. Chem. Chem. Phys., 2019, 21, 8559–8568.

36 A. Sahoo and S. Matysiak, Effects of applied surface-tension on membrane-assisted Ab aggregation, Phys. Chem. Chem. Phys., 2021, 23, 20627–20633.

37 S. O. Yesylevskyy, L. V. Schafer, D. Sengupta and S. J. Marrink, PolarizableWater Model for the Coarse-Grained MARTINI Force Field, PLoS Comput. Biol., 2010, 6, e1000810.

38 B. K. Mueller, S. Subramaniam and A. Senes, A frequent, GxxxG-mediated, transmembrane association motif is optimized for the formation of interhelical Ca–H hydrogen bonds, Proc. Natl. Acad. Sci. U. S. A., 2014, 111, E888–E895.

39 A. R. Curran and D. M. Engelman, Sequence motifs, polar interactions and conformational changes in helical membrane proteins, Curr. Opin. Struct. Biol., 2003, 13, 412–417.

40 M. J. Abraham, T. Murtola, R. Schulz, S. Pall, J. C. Smith, B. Hess and E. Lindahl, GROMACS: High performance molecular simulations through multi-level parallelism from laptops to supercomputers, SoftwareX, 2015, 1–2, 19–25.

41 W. Humphrey, A. Dalke and K. Schulten, VMD: visual molecular dynamics, J. Mol. Graphics, 1996, 14, 33–38.

42 T. Darden, D. York and L. Pedersen, Particle mesh Ewald: An Nlog(N) method for Ewald sums in large systems, J. Chem. Phys., 1993, 98, 10089–10092.

43 U. Essmann, L. Perera, M. L. Berkowitz, T. Darden, H. Lee and L. G. Pedersen, A smooth particle mesh Ewald method, J. Chem. Phys., 1995, 103, 8577–8593.

44 H. A. Posch, W. G. Hoover and F. J. Vesely, Canonical dynamics of the Nose oscillator: Stability, order, and chaos, Phys. Rev. A: At., Mol., Opt. Phys., 1986, 33, 4253–4265.

45 Y. Zhang, D. W. Kulp, J. D. Lear and W. F. DeGrado, Experimental and computational evaluation of forces directing the association of transmembrane helices, J. Am. Chem. Soc., 2009, 131, 11341–11343.

46 M. Mottamal, J. Zhang and T. Lazaridis, Energetics of the native and non-native states of the glycophorin transmembrane helix dimer, Proteins: Struct., Funct., Genet., 2006, 62, 996–1009.

47 K. R. MacKenzie and D. M. Engelman, Structure-based prediction of the stability of transmembrane helix–helix interactions: the sequence dependence of glycophorin A dimerization, Proc. Natl. Acad. Sci. U. S. A., 1998, 95, 3583–3590.

48 D. Dell'Orco, P. G. De Benedetti and F. Fanelli, In silico screening of mutational effects on transmembrane helix dimerization: insights from rigid-body docking and molecular dynamics simulations, J. Phys. Chem. B, 2007, 111, 9114–9124.

49 K. G. Fleming, A. L. Ackerman and D. M. Engelman, The effect of point mutations on the free energy of transmembrane a-helix dimerization, J. Mol. Biol., 1997, 272, 266–275.

This journal is © the Owner Societies 2023

Phys. Chem. Chem. Phys., 2023, 25, 10885–10893 | 10893